

EarthBridge: A Solution for 4th Multi-modal Aerial View Image Challenge Translation Track

Zhenyuan Chen[†], Yuanshen Guan[†], Feng Zhang[‡]

ZJU USTC ZJU

bili_sakura@zju.edu.cn guanys@mail.ustc.edu.cn zfcarnation@zju.edu.cn*

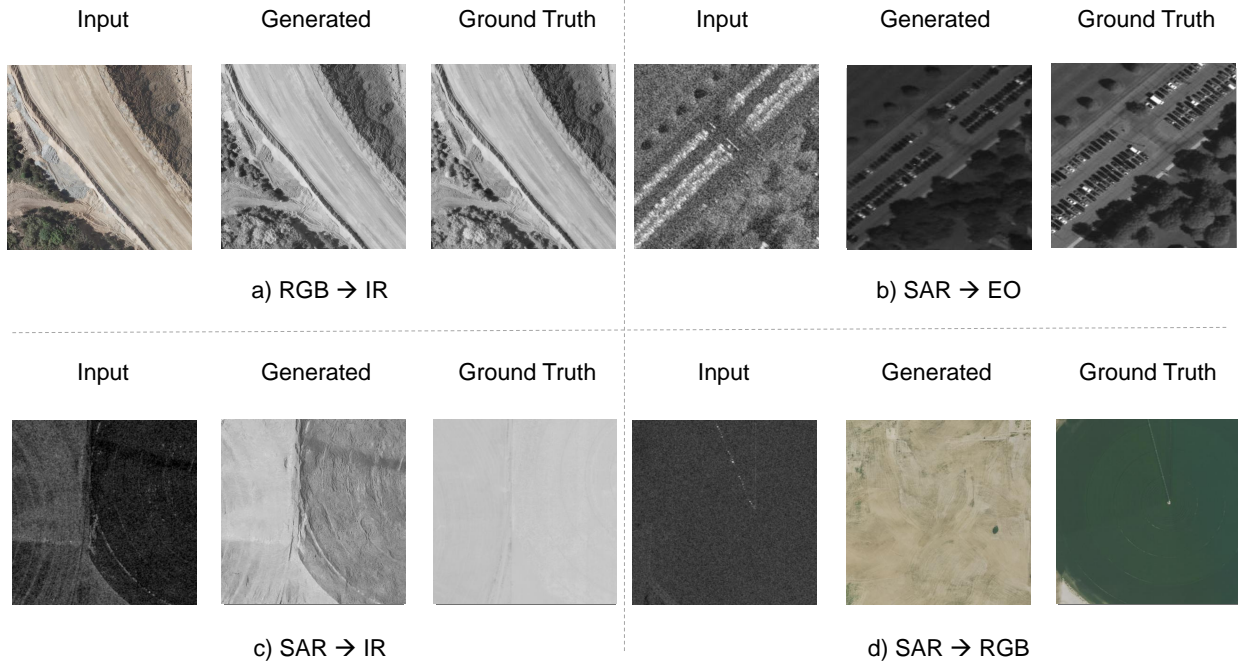


Figure 1. Qualitative results on our hold-out validation set from the official train set. (a) RGB→IR, (b) SAR→EO, (c) SAR→IR, (d) SAR→RGB. Each panel shows input, generated output, and ground-truth target. EarthBridge preserves structural integrity while synthesizing high-fidelity textures across Electro-Optical (EO), Infrared (IR), and Synthetic Aperture Radar (SAR) modalities.

Abstract

Cross-modal image-to-image translation among Electro-Optical (EO), Infrared (IR), and Synthetic Aperture Radar (SAR) sensors is essential for comprehensive multi-modal aerial-view analysis. However, translating between these modalities is notoriously difficult due to their distinct

electromagnetic signatures and geometric characteristics. This paper presents **EarthBridge**, a high-fidelity translation framework developed for the 4th Multi-modal Aerial View Image Challenge – Translation (MAVIC-T). We explore two distinct methodologies: **Diffusion Bridge Implicit Models (DBIM)**, which we generalize using non-Markovian bridge processes for high-quality deterministic sampling, and **Contrastive Unpaired Trans-**

*Equal contribution (†). Corresponding author (‡).

lation (CUT), which utilizes contrastive learning for structural consistency. Our EarthBridge framework employs a channel-concatenated UNet denoiser trained with Karras-weighted bridge scalings and a specialized "booting noise" initialization to handle the inherent ambiguity in cross-modal mappings. We evaluate these methods across all four challenge tasks (SAR→EO, SAR→RGB, SAR→IR, RGB→IR), achieving superior spatial detail and spectral accuracy. Our solution achieved a composite score of 0.38, securing the second position on the MAVIC-T leaderboard. Code is available at <https://github.com/Bili-Sakura/EarthBridge-Preview>.

1 Introduction

The Multi-modal Aerial View Image Challenge for cross-domain image translation [2, 23, 24] is a leading challenge held in conjunction with the Perception Beyond the Visible Spectrum (PBVS) workshop from 2023 to 2025. Data collected across multiple sensing modalities—such as Electro-Optical (EO), Infrared (IR), and Synthetic Aperture Radar (SAR)—provide complementary perspectives on the same scene. However, data coverage limitations and modality-specific constraints often hinder the full utilization of these diverse sources. For instance, while SAR sensors offer all-weather capabilities and can penetrate atmospheric obstructions, their imagery is complex to interpret, and publicly available datasets are scarce. Conversely, widely available EO imagery is limited by lighting conditions and atmospheric visibility. Domain translation seeks to bridge this gap by converting one modality into another, enabling cross-modal data synthesis and enhancing sensor interoperability. By focusing on translation tasks such as RGB→IR, SAR→EO, SAR→IR, and SAR→RGB, the MAVIC-T challenge aims to bolster existing data volume, increase data diversity across regions, and serve as a platform for advancing conditioned image synthesis techniques, ultimately fostering the development of more adaptable and robust models for multi-modal image analysis.

SAR images possess unique attributes that present challenges for both human observers and vision artificial intelligence (AI) models to interpret, owing to their electromagnetic (EM) characteristics [14–17, 25].

In this paper, we propose **EarthBridge**, a multi-method framework for cross-modal aerial image translation. Our primary approach is built on Diffusion Bridge Implicit Models (DBIM) [54], which we generalize with non-Markovian bridge processes to enable efficient deterministic sampling. In parallel, we explore Contrastive Unpaired Translation (CUT) [29] as a powerful contrastive-learning-based alternative. Unlike standard conditional diffusion models that diffuse targets to pure noise and rely on classifier-free guidance or simple concatenation for the reverse path, EarthBridge implements a genuine stochastic diffusion bridge. By directly constraining the forward generative trajectory between the source modality x_T and target modality x_0 , and parameterizing the UNet denoiser to solve the bridge marginals under Karras-weighted scalings [19], EarthBridge (DBIM) achieves high-fidelity translation across disparate modalities. We utilize pixel-level modeling throughout both approaches to preserve the full spectral and spatial resolution of the remote sensing data.

Our findings indicate that the deterministic DBIM sampling significantly improves inference speed, achieving high-quality results in as few as 5 sampling steps in RGB→IR. Qualitatively, EarthBridge demonstrates a superior ability to reconstruct complex urban layouts and fine-grained textures in challenging tasks such as SAR-to-RGB, effectively bridging the domain gap. Quantitatively, our solution achieves a composite task score of 0.269 for the SAR→EO task and 0.38 overall, ultimately placing second in the MAVIC-T challenge leaderboard.

Our main contributions are summarized as follows:

- We propose **EarthBridge**, a multi-method framework for paired cross-modal aerial image translation incorporating both Diffusion Bridge Implicit Models (DBIM) and Contrastive Unpaired Translation (CUT), providing a robust comparison between diffusion-based and contrastive-learning-based approaches.
- We develop a specialized training protocol using Karras-weighted bridge scalings and pixel-level modeling, optimized for the high dynamic range and resolution requirements of multimodal remote sensing data.
- We conduct comprehensive experiments on all four MAVIC-T tasks (SAR→EO, SAR→RGB, SAR→IR, RGB→IR), reporting competitive results and providing detailed quantitative and qualitative analysis.

2 Related Work

Translating across remote sensing (RS) modalities, such as SAR to optical (S2O), is critical for multisource data fusion. In this section, we provide a comprehensive literature review of image-to-image translation, diffusion bridge models, and cross-modality translation to complement the specialized discussion on remote sensing.

Image-to-Image and Cross-Modality Translation.

Image-to-image translation has been extensively studied in computer vision. Foundational works include Pix2Pix for paired conditional translation [18] and CycleGAN for unpaired translation [56]. Subsequent advances include contrastive learning for unpaired translation [29], zero-shot [30] and one-step translation with text-to-image models [31]. Translation across diverse sensor modalities—grayscale, near-infrared (NIR), thermal colorization, and color transfer—has been addressed with probabilistic color correction [28], NIR imagery colorization [41], and deep colorization [25, 50].

Diffusion Bridge Models. Unlike standard diffusion models that generate from noise, diffusion bridge models learn a stochastic process that directly connects source and target distributions, making them well-suited for paired image-to-image translation. Denoising Diffusion Bridge Models (DDBM) [55] define a variance-preserving bridge between data distributions. Related formulations include Brownian Bridge Diffusion Models (BBDM) [20] and its bidirectional extension BiBBDM [46], Image-to-Image Schrödinger Bridge (I²SB) [21], Diffusion Schrödinger Bridge matching [39], Dual Diffusion Implicit Bridges [40], and Direct Diffusion Bridge with data consistency [5]. Recent extensions include Consistency Diffusion Bridge [9], Diffusion Bridge Implicit Models [54], Latent Bridge Matching for fast translation [3], deterministic translation via denoising Brownian bridge with dual approximators [45], and adaptive domain shift for cross-modality translation [44].

RS Image to Image Translation. SAR-to-optical (S2O) translation bridges heterogeneous sensor data for multisource fusion. GAN-based works include hierarchical latent features [43], fire-disturbed region recon-

struction [13], DINO-driven optical priors [10], hybrid ViT-cGANs [53], and semi-supervised multi-scale matching [47]. Diffusion models now dominate: conditional diffusion with spatial-frequency refinement [1, 33], one-step translation [34], robust layout-based iterative refinement [52], adaptive domain shift [44], and Any2Any with DiT for arbitrary modality translation [4]. Broader image translation methods such as CSHNet [48] address information asymmetry across modalities.

3 Preliminary

Problem Formulation Let $\mathcal{X} \subset \mathbb{R}^{C_s \times H \times W}$ denote the source domain and $\mathcal{Y} \subset \mathbb{R}^{C_t \times H \times W}$ denote the target domain, where C_s and C_t are the number of channels in the source and target modalities, respectively. Given a set of spatially-aligned training pairs $\{(x_i, y_i)\}_{i=1}^N$ with $x_i \in \mathcal{X}$ and $y_i \in \mathcal{Y}$, the goal of cross-modal image-to-image translation is to learn a mapping $G : \mathcal{X} \rightarrow \mathcal{Y}$ that minimizes a composite distance between the generated image $\hat{y} = G(x)$ and the ground-truth target y . In the context of the MAVIC-T challenge, four translation tasks are defined (see Tab. 1): SAR→EO (1→1 channel, 256×256), SAR→RGB (1→3, 1024×1024), SAR→IR (1→1, 1024×1024), and RGB→IR (3→1, 1024×1024).

Evaluation Metric The MAVIC-T challenge evaluates submissions using a composite score derived from three complementary metrics: LPIPS [51] (Learned Perceptual Image Patch Similarity, based on VGG-16) for perceptual fidelity, FID [12] (Fréchet Inception Distance, based on InceptionV3) for distributional similarity, and L1 norm for pixel-level structural accuracy. These are combined into a task score:

$$S_{\text{task}} = \frac{\frac{2}{\pi} \arctan(\text{FID}) + \text{LPIPS} + \text{L1}}{3}, \quad (1)$$

where the arctan normalization maps FID into the [0, 1] range to balance its contribution against the other two metrics. The overall score is the average of the four task scores, with a penalty of +1 added for each unattempted domain, encouraging participants to develop generalizable solutions across all modality pairs.

4 EarthBridge

We propose EarthBridge, built on Diffusion Bridge Implicit Models (DBIM) [54] for high-fidelity cross-modal translation. We also include Contrastive Unpaired Translation (CUT) [29] as a supplementary baseline for comparison.

4.1 Diffusion Bridge Implicit Models (DBIM)

Diffusion models have recently revolutionized generative modeling, yet they are fundamentally designed to transport complex distributions to a standard Gaussian prior. Adapting them to translate between two arbitrary distributions, such as heterogeneous remote sensing modalities, requires conditioning the diffusion process on a fixed endpoint. This is achieved via Doob’s h -transform [8, 35].

Stochastic Bridges via h -transform. Given a base diffusion process $dx_t = f(x_t, t)dt + g(t)dw_t$, the conditioned SDE that almost surely reaches a prescribed target $x_0 = y$ at $t = 0$ starting from a source $x_T = x$ at $t = T$ is given by:

$$dx_t = f(x_t, t)dt + g(t)dw_t + g(t)^2 \nabla_{x_t} \log p(x_0 = y | x_t)dt, \quad (2)$$

where $p(x_0 = y | x_t)$ is the transition density of the original process. When the endpoints are fixed, the resulting conditioned process is called a *diffusion bridge* [6, 11, 22, 32, 37, 38], which forms the foundational mechanism for transporting one state to another. In the context of cross-modal translation, x represents the source modality (e.g., SAR) and y the target modality (e.g., optical). This formulation ensures that the generative trajectory is directly constrained by both endpoints, providing a more principled framework for paired translation than standard conditional diffusion.

Denosing Diffusion Bridge Models. Denoising Diffusion Bridge Models (DDBM) [55] provide a tractable realization of Eq. 2. Under a variance-preserving (VP) schedule, the forward bridge process constructs intermediate states z_t as:

$$z_t = a_t x + b_t y + \sigma_t \epsilon, \quad \epsilon \sim \mathcal{N}(0, I), \quad (3)$$

where a_t, b_t, σ_t are schedule-dependent coefficients. While DDBM excels in high-fidelity generation, its inference typically relies on simulating Eq. 2 via computationally expensive numerical solvers (e.g., Heun or stochastic samplers), often requiring hundreds of function evaluations (NFE) for optimal results. In this work, we adopt the more efficient *implicit* formulation to accelerate this process. Fig. 2 illustrates the distribution evolution from source to target.

4.2 EarthBridge: Non-Markovian DBIM

We present our DBIM approach which generalizes the diffusion bridge framework with non-Markovian bridge processes defined on discretized timesteps. Our solution leverages the deterministic sampling property of DBIM to achieve high-fidelity cross-modal translation with significantly fewer sampling steps compared to the vanilla DDBM. Figs. 3 and 4 show our sampling procedure and the UNet architecture.

Non-Markovian Diffusion Bridges. In contrast to the continuous-time Markovian bridge processes in DDBM, we consider a family of non-Markovian diffusion bridges defined over a sequence of discretized timesteps $0 = t_0 < t_1 < \dots < t_N = T$, controlled by a variance parameter $\rho \in \mathbb{R}^{N-1}$. The UNet denoiser is trained to predict the bridge marginals governed by the schedule-dependent coefficients (a_t, b_t, c_t) , where the source image \mathbf{x} is supplied to the network via channel concatenation. This concatenation is strictly an architectural mechanism to inject the mandatory endpoint parameter \mathbf{x} into the SDE formulation, not an ad-hoc conditioning trick akin to standard image-to-image models. The joint probability distribution $q^{(\rho)}(\mathbf{z}_{t_0:N-1} | \mathbf{x})$ is factorized through a chain of conditional distributions:

$$q^{(\rho)}(\mathbf{z}_{t_0:N-1} | \mathbf{x}) = q_0(\mathbf{z}_{t_0}) \prod_{n=1}^{N-1} q^{(\rho)}(\mathbf{z}_{t_n} | \mathbf{z}_0, \mathbf{z}_{t_{n+1}}, \mathbf{x}), \quad (4)$$

where q_0 is the target modality distribution and each step $q^{(\rho)}$ is defined as:

$$\mathcal{N}(a_{t_n} \mathbf{x} + b_{t_n} \mathbf{z}_0 + \sqrt{c_{t_n}^2 - \rho_n^2} \boldsymbol{\eta}_{n+1}, \rho_n^2 \mathbf{I}), \quad (5)$$

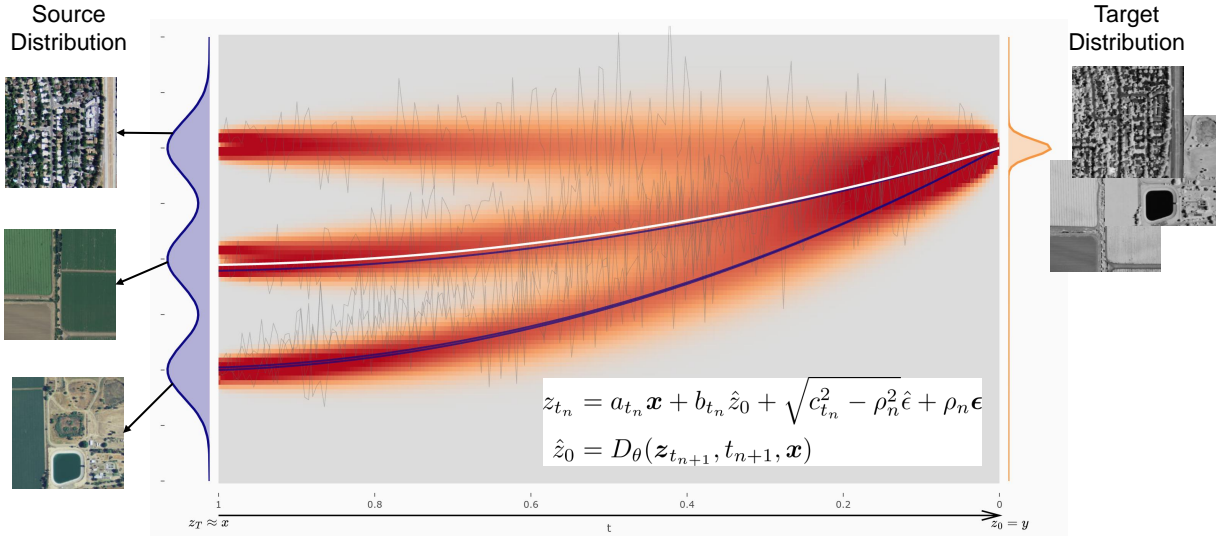


Figure 2. Distribution evolution of the diffusion bridge. The source distribution at $z_T = \mathbf{x}$ (left) converges through time t to the target distribution at $z_0 = \mathbf{y}$ (right), governed by the DBIM update rule and denoiser D_θ .

with $\boldsymbol{\eta}_{n+1} = (\mathbf{z}_{t_{n+1}} - a_{t_{n+1}} \mathbf{x} - b_{t_{n+1}} \mathbf{z}_0) / c_{t_{n+1}}$. Here, a_t, b_t, c_t are known coefficients determined by the VP log-SNR schedule (Sec. 4.1). Under this construction, the marginal distributions $q^{(\rho)}(\mathbf{z}_{t_n} | \mathbf{x})$ are preserved to be consistent with the continuous-time forward bridge (Eq. (3)). The variance parameter ρ controls the level of stochasticity in the sampling process, ranging from a purely Markovian stochastic process to a fully deterministic implicit model.

Reverse Generative Process and Sampling. The generative process is initialized at the source image $z_T = \mathbf{x}$ and iteratively samples z_{t_n} from $z_{t_{n+1}}$ via a parameterized data predictor $D_\theta(z_{t_{n+1}}, t_{n+1}, \mathbf{x})$. The core updating rule is given by:

$$z_{t_n} = a_{t_n} \mathbf{x} + b_{t_n} \hat{z}_0 + \sqrt{c_{t_n}^2 - \rho_n^2} \hat{\epsilon} + \rho_n \epsilon, \quad (6)$$

where $\hat{z}_0 = D_\theta(z_{t_{n+1}}, t_{n+1}, \mathbf{x})$ is the clean data prediction and $\hat{\epsilon}$ is the predicted noise at time t_{n+1} . Setting $\rho_n = 0$ for all steps yields the deterministic *Diffusion Bridge Implicit Model (DBIM)*, which can be viewed as an Euler discretization of a probability flow ODE specifically tailored for diffusion bridges.

Booting Noise. A critical refinement in our sampling procedure is the introduction of *booting noise* at the initial step ($t_N = T$). Since $c_{t_N} = 0$, the denominator in $\hat{\epsilon}$ leads to singularity. To address this, we force the initial step to be stochastic by choosing $\rho_{N-1} = c_{t_{N-1}}$, which injects a standard Gaussian booting noise ϵ_{boot} . This booting noise serves as the latent variable, encoding the one-to-many mapping ambiguity in RS translation (e.g., several plausible infrared images for a single SAR input).

Channel Handling for Mismatched Modalities. For tasks where source and target modalities have different channel counts (e.g., RGB→IR or SAR→RGB), we operate the bridge in a shared model channel space (typically 3 for RGB-related tasks). Single-band modalities are expanded to model channels by channel repetition before entering the UNet, ensuring the concatenation $[z_t, \mathbf{x}]$ remains well-defined across all tasks.

4.3 Contrastive Unpaired Translation (CUT) — Supplementary

As a supplementary baseline, we use CUT [29] for the SAR→IR task. Unlike diffusion bridges, CUT is a feed-

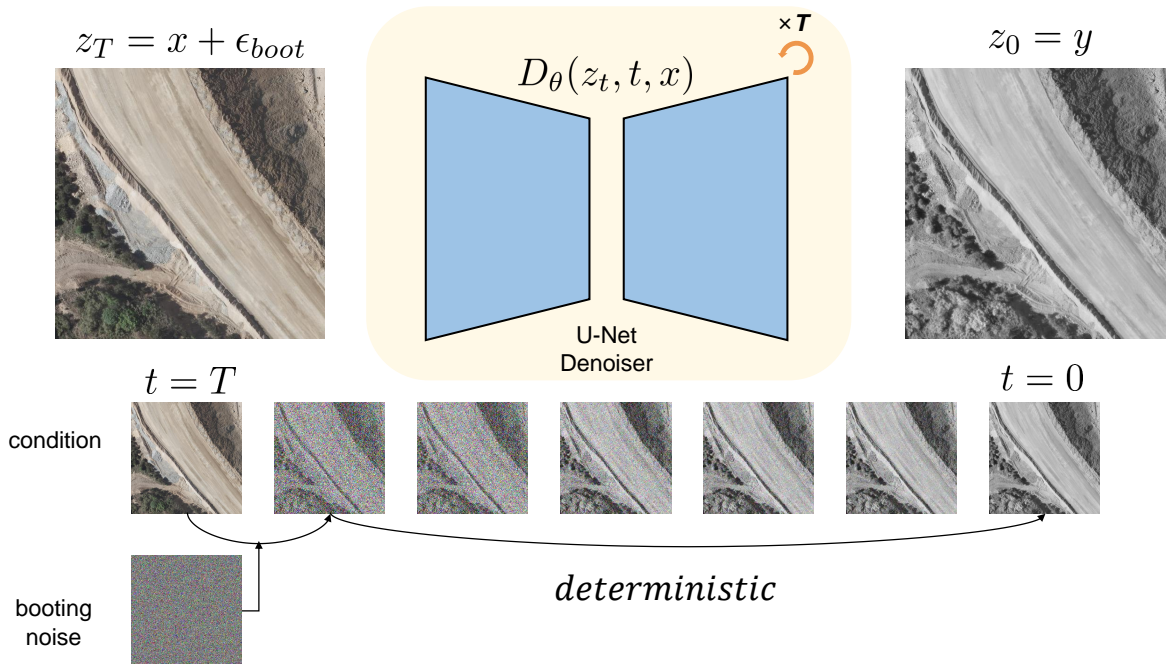


Figure 3. Deterministic DBIM sampling. The noisy input $z_T = x + \epsilon_{boot}$ is progressively denoised by $D_\theta(z_t, t, x)$ to produce the clean output $z_0 = y$. The step sequence shows conditioning, booting noise injection, and gradual refinement from $t = T$ to $t = 0$.

forward GAN that performs translation in a single forward pass. It combines an adversarial loss with a patch-based contrastive loss to maintain structural correspondence between source and output. Architecture and hyperparameter details are in Sec. 6.1.

PatchNCE Loss. CUT extracts multi-layer encoder features from both the source x and the generated image $\hat{y} = G(x)$. A lightweight MLP samples spatial patches per layer, projects them to an embedding space, and applies L2 normalization. The PatchNCE (InfoNCE [42]) loss encourages that the query embedding from a patch in \hat{y} is closer to the key embedding from the corresponding patch in x than to embeddings from other patches. Formally, for query q and key k at the same spatial location, the loss uses $\ell_{NCE} = -\log \frac{\exp(q^\top k/\tau)}{\exp(q^\top k/\tau) + \sum_{k'} \exp(q^\top k'/\tau)}$, with temperature τ and negatives k' from other patches. This contrastive objective preserves structural layout across the translation.

Training Objective. The generator minimizes $\mathcal{L}_G = \lambda_{GAN} \mathcal{L}_{GAN} + \lambda_{NCE} \mathcal{L}_{NCE}$, where \mathcal{L}_{GAN} is the LSGAN [26] objective (generator encourages the discriminator to classify $G(x)$ as real) and \mathcal{L}_{NCE} is the per-layer PatchNCE loss averaged over the selected encoder layers.

5 Experiments

5.1 Dataset and Preprocessing

We use the MAVIC-T 2025 dataset from the challenge organizers, with imagery from UNICORN, USGS EROS HRO, and UMBRA across four regions: Bingham, Centerfield, Manhattan, and UC Davis. We do not use any external datasets beyond the official challenge data. Tab. 1 summarizes the four translation tasks. SAR→EO operates at 256×256 ; the other three tasks use 1024×1024 . For SAR→IR and SAR→RGB, we spatially align SAR scenes with optical mosaics before resampling. We also

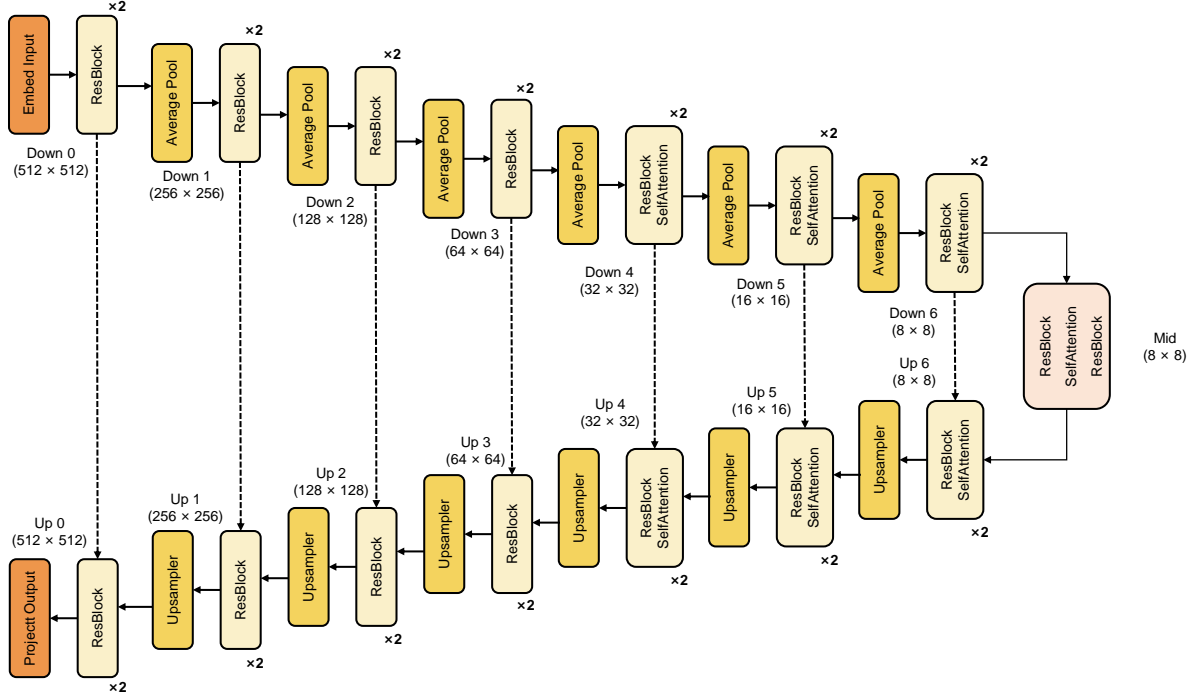


Figure 4. UNet denoiser architecture for 1024px tasks (SAR→RGB, RGB→IR). The encoder downsamples via ResBlocks and average pooling; the decoder upsamples with skip connections. Source x is channel-concatenated with z_t ; the output is \hat{z}_0 . We train at 512×512 and infer at full resolution.

Table 1. Task specifications and training data for the MAVIC-T challenge. Crop augmentation uses 1024×1024 sliding windows with stride 512 (50% overlap); SAR→optical pairs are georeference-aligned.

Task	Resolution	Channels	Samples (Orig.)	Samples (Aug.)
SAR→EO	256×256	1→1	89,411	–
SAR→RGB	1024×1024	1→3	10,576	75,703
SAR→IR	1024×1024	1→1	10,576	74,317
RGB→IR	1024×1024	3→1	2,272	7,388

create crop-augmented training sets for the 1024×1024 tasks to increase data diversity.

5.2 Architecture and Training Objectives

Design Choice For DBIM-based tasks (SAR→EO, SAR→RGB, RGB→IR), we use a UNet [36] denoiser that predicts the clean target from the noisy sample conditioned on timestep and source image. For SAR→IR, we adopt CUT [29] as an alternative baseline, exploiting

its patch-based contrastive learning for structural consistency. Per-task architectural and hyperparameter choices are summarized in Tab. 4.

Training Objective For DBIM, the primary training objective is a weighted mean squared error between the denoised prediction and the clean target:

$$\mathcal{L}_{\text{denoise}} = \mathbb{E}_{(x,y), t, \epsilon} [w(t) \cdot \|D_{\theta}(z_t, t, x) - y\|_2^2], \quad (7)$$

where $w(t)$ is the Karras bridge weighting. Diffusion time t is sampled from a Karras inverse- ρ distribution; inference uses deterministic DBIM sampling. Full technical details on architecture, schedule, and per-task configurations are in Sec. 6.1.

5.3 Quantitative Results

Tab. 2 presents the quantitative performance comparison between EarthBridge and the CUT baseline across the

Table 2. Main results on the MAVIC-T evaluation set. \downarrow lower is better. Time is per-sample inference latency; SAR \rightarrow EO is run at 256px with large batch size, and its latency is averaged.

Track	Method	FID \downarrow	LPIPS \downarrow	L1 \downarrow	Score \downarrow	NFE	Time
SAR \rightarrow EO	DBIM	0.22	0.50	0.08	0.27	500	0.42 s
SAR \rightarrow RGB	DBIM	0.88	0.64	0.21	0.58	1000	160 s
SAR \rightarrow IR	CUT	0.65	0.60	0.15	0.46	1	0.47 s
RGB \rightarrow IR	DBIM	0.36	0.15	0.09	0.20	5	1.5 s

Table 3. Leaderboard comparison. Per-task scores (SAR \rightarrow EO, SAR \rightarrow RGB, SAR \rightarrow IR, RGB \rightarrow IR) from the challenge evaluation.

Rank	Participant	SAR \rightarrow EO	SAR \rightarrow RGB	SAR \rightarrow IR	RGB \rightarrow IR	Combined
1st	wangzhiyu918	0.11	0.50	0.49	0.20	0.32
2nd	EarthBridge (Ours)	<u>0.27</u>	<u>0.58</u>	0.46	0.20	<u>0.38</u>

challenge tasks. Tab. 3 compares our second-place submission with the first-place result (wangzhiyu918); note that lower scores indicate better performance (the official leaderboard display was initially reversed). The composite task score provides a balanced evaluation of perceptual, distributional, and structural fidelity. EarthBridge demonstrates consistent performance across both low- and high-resolution tasks.

5.4 Qualitative Results

Fig. 5 (appendix) shows qualitative examples across all four tasks. EarthBridge preserves fine-grained structural information from the source modality while accurately synthesizing target textures, demonstrating consistent performance across both low- and high-resolution settings.

6 Implementation Details

This section provides the comprehensive technical details of the EarthBridge architecture, training hyperparameters, and multi-modal refinement modules. We use the Prodigy optimizer [27] for all training. Training employs mixed precision in BF16; inference is also run in BF16.

6.1 Architecture, Sampling, and Scheduler Settings

DBIM. The denoiser uses an ADM-style UNet [7]. Source conditioning is via channel-wise concatenation $[z_t, x]$. For SAR \rightarrow RGB, we use REPA [49] in our implementation, which relieves the loss spike issue in the early training steps. Sampling follows the deterministic DBIM formulation [54] with task-dependent inference steps (Tab. 2) and Gaussian booting noise ϵ_{boot} at $t = T$. Tab. 4 summarizes per-task architectural and training configurations, including the VP log-SNR schedule and Karas diffusion-time sampling.

CUT. The CUT formulation (PatchNCE loss, training objective) is described in Sec. 4.3. Our implementation follows the original architecture [29] with three core components: a ResNet-based generator, a PatchGAN [18] discriminator, and a PatchSampleMLP for patch-wise contrastive learning. Tab. 4 summarizes per-task architectural and training configurations.

References

- [1] Xinyu Bai, Xinyang Pu, and Feng Xu. Conditional Diffusion for SAR to Optical Image Translation. *IEEE Geoscience and Remote Sensing Letters*, 21: 1–5, 2024.
- [2] Dylan Bowald, Justice Wheelwright, Oliver Nina, Angel Sappa, Riad Hammoud, Erik Blasch, and Nathan Inkawhich. 3rd Multi-modal Aerial View Image Challenge: Sensor Domain Translation - PBVS 2025. In *Proceedings of the IEEE/CVF Conference on Computer Vision and Pattern Recognition*, pages 4679–4688, 2025.
- [3] Clément Chadebec, Onur Tasar, Sanjeev Sreetharan, and Benjamin Aubin. LBM: Latent Bridge Matching for Fast Image-to-Image Translation. In *Proceedings of the IEEE/CVF International Conference on Computer Vision*, pages 29086–29098, 2025.
- [4] Haoyang Chen, Jing Zhang, Hebaixu Wang, Shiqin Wang, Pohsun Huang, Jiayuan Li, Haonan Guo, Di Wang, Zheng Wang, and Bo Du. Any2Any: Unified Arbitrary Modality Translation for Remote Sensing, 2026.
- [5] Hyungjin Chung, Jeongsol Kim, and Jong Chul Ye. Direct Diffusion Bridge using Data Consistency for Inverse Problems. In *Neural Information Processing Systems*, pages 7158–7169. Curran Associates, Inc., 2023.
- [6] Bernard Delyon and Ying Hu. Simulation of conditioned diffusion and application to parameter estimation. *Stochastic Processes and Their Applications*, 116(11):1660–1675, 2006.
- [7] Prafulla Dhariwal and Alexander Nichol. Diffusion Models Beat GANs on Image Synthesis. In *Advances in Neural Information Processing Systems*, pages 8780–8794. Curran Associates, Inc., 2021.
- [8] Joseph L. Doob and J. I. Doob. *Classical Potential Theory and Its Probabilistic Counterpart*. Springer, 1984.
- [9] Guande He, Kaiwen Zheng, Jianfei Chen, Fan Bao, and Jun Zhu. Consistency Diffusion Bridge Models. In *The Thirty-eighth Annual Conference on Neural Information Processing Systems*, 2024.
- [10] Jingfei He, Liang Chen, Hao Shi, Yuhang Chen, Jingyi Yang, and Wei Li. DOGAN: DINO-Based Optical-Prior-Driven GAN for SAR-to-Optical Image Translation. *IEEE Transactions on Geoscience and Remote Sensing*, 63:1–16, 2025.
- [11] Jeremy Heng, Valentin De Bortoli, Arnaud Doucet, and James Thornton. Simulating diffusion bridges with score matching. *arXiv preprint arXiv:2111.07243*, 2021.
- [12] Martin Heusel, Hubert Ramsauer, Thomas Unterthiner, Bernhard Nessler, and Sepp Hochreiter. GANs Trained by a Two Time-Scale Update Rule Converge to a Local Nash Equilibrium. In *Advances in Neural Information Processing Systems*. Curran Associates, Inc., 2017.
- [13] Xikun Hu, Puzhao Zhang, and Yifang Ban. Gan-based SAR to Optical Image Translation in Fire-Disturbed Regions. In *IGARSS 2022 - 2022 IEEE International Geoscience and Remote Sensing Symposium*, pages 1456–1459, 2022.
- [14] Zhongling Huang, Mihai Datcu, Zongxu Pan, and Bin Lei. Deep SAR-Net: Learning objects from signals. *ISPRS Journal of Photogrammetry and Remote Sensing*, 161:179–193, 2020.
- [15] Zhongling Huang, Mihai Datcu, Zongxu Pan, Xiaolan Qiu, and Bin Lei. HDEC-TFA: An Unsupervised Learning Approach for Discovering Physical Scattering Properties of Single-Polarized SAR Image. *IEEE Transactions on Geoscience and Remote Sensing*, 59(4):3054–3071, 2021.
- [16] Zhongling Huang, Corneliu Octavian Dumitru, Zongxu Pan, Bin Lei, and Mihai Datcu. Classification of Large-Scale High-Resolution SAR Images With Deep Transfer Learning. *IEEE Geoscience and Remote Sensing Letters*, 18(1):107–111, 2021.
- [17] Zhongling Huang, Xiwen Yao, Ying Liu, Corneliu Octavian Dumitru, Mihai Datcu, and Junwei Han. Physically explainable CNN for SAR image classification. *ISPRS Journal of Photogrammetry and Remote Sensing*, 190:25–37, 2022.
- [18] Phillip Isola, Jun-Yan Zhu, Tinghui Zhou, and Alexei A. Efros. Image-To-Image Translation With Conditional Adversarial Networks. In *Proceedings of the IEEE Conference on Computer Vision and Pattern Recognition*, pages 1125–1134, 2017.
- [19] Tero Karras, Miika Aittala, Timo Aila, and Samuli Laine. Elucidating the design space of diffusion-

- based generative models. In *Adv. Neural Inform. Process. Syst.*, 2022.
- [20] Bo Li, Kaitao Xue, Bin Liu, and Yu-Kun Lai. BBDM: Image-to-image translation with brownian bridge diffusion models. In *Proceedings of the IEEE/CVF Conference on Computer Vision and Pattern Recognition (CVPR)*, pages 1952–1961, 2023.
- [21] Guan-Hong Liu, Arash Vahdat, De-An Huang, Evangelos Theodorou, Weili Nie, and Anima Anandkumar. I²sb: Image-to-Image Schrödinger Bridge. In *The Eleventh International Conference on Learning Representations*, 2023.
- [22] Xingchao Liu, Lemeng Wu, Mao Ye, and Qiang Liu. Let us build bridges: Understanding and extending diffusion generative models. *arXiv preprint arXiv:2208.14699*, 2022.
- [23] Spencer Low, Oliver Nina, Angel D. Sappa, Erik Blasch, and Nathan Inkawhich. Multi-modal Aerial View Image Challenge: Translation from Synthetic Aperture Radar to Electro-Optical Domain Results - PBVS 2023. In *2023 IEEE/CVF Conference on Computer Vision and Pattern Recognition Workshops (CVPRW)*, pages 515–523, 2023.
- [24] Spencer Low, Oliver Nina, Dylan Bowald, Angel D. Sappa, Nathan Inkawhich, and Peter Bruns. Multi-modal Aerial View Image Challenge: Sensor Domain Translation. In *Proceedings of the IEEE/CVF Conference on Computer Vision and Pattern Recognition*, pages 3096–3104, 2024.
- [25] Uttam K Majumder, Erik P Blasch, and David A Garren. *Deep learning for radar and communications automatic target recognition*. Artech House, 2020.
- [26] Xudong Mao, Qing Li, Haoran Xie, Raymond Y.K. Lau, Zhen Wang, and Stephen Paul Smolley. Least squares generative adversarial networks. In *Proceedings of the IEEE International Conference on Computer Vision (ICCV)*, 2017.
- [27] Konstantin Mishchenko and Aaron Defazio. Prodigy: An Exponentially Adaptive Parameter-Free Learner. In *Proceedings of the 41st International Conference on Machine Learning*, pages 35779–35804. PMLR, 2024.
- [28] Miguel Oliveira, Angel Domingo Sappa, and Vitor Santos. A Probabilistic Approach for Color Correction in Image Mosaicking Applications. *IEEE Transactions on Image Processing*, 24(2):508–523, 2015.
- [29] Taesung Park, Alexei A. Efros, Richard Zhang, and Jun-Yan Zhu. Contrastive Learning for Unpaired Image-to-Image Translation. In *Computer Vision–ECCV 2020: 16th European Conference, Glasgow, UK, August 23–28, 2020, Proceedings, Part IX 16*, pages 319–345, Cham, 2020. Springer International Publishing.
- [30] Gaurav Parmar, Krishna Kumar Singh, Richard Zhang, Yijun Li, Jingwan Lu, and Jun-Yan Zhu. Zero-shot Image-to-Image Translation. In *ACM SIGGRAPH 2023 Conference Proceedings*, pages 1–11, New York, NY, USA, 2023. Association for Computing Machinery.
- [31] Gaurav Parmar, Taesung Park, Srinivasa Narasimhan, and Jun-Yan Zhu. One-Step Image Translation with Text-to-Image Models, 2024.
- [32] Stefano Peluchetti. Non-denoising forward-time diffusions. *arXiv preprint arXiv:2109.11704*, 2021.
- [33] Jiang Qin, Kai Wang, Bin Zou, Lamei Zhang, and Joost van de Weijer. Conditional Diffusion Model With Spatial-Frequency Refinement for SAR-to-Optical Image Translation. *IEEE Transactions on Geoscience and Remote Sensing*, 62:1–14, 2024.
- [34] Jiang Qin, Bin Zou, Haolin Li, and Lamei Zhang. Efficient End-to-End Diffusion Model for One-Step SAR-to-Optical Translation. *IEEE Geoscience and Remote Sensing Letters*, 22:1–5, 2025.
- [35] L. Chris G. Rogers and David Williams. *Diffusions, Markov Processes and Martingales: Volume 2, Itô Calculus*. Cambridge University Press, 2000.
- [36] Olaf Ronneberger, Philipp Fischer, and Thomas Brox. U-Net: Convolutional Networks for Biomedical Image Segmentation. In *Medical Image Computing and Computer-Assisted Intervention – MICCAI 2015*, pages 234–241, Cham, 2015. Springer.
- [37] Simo Särkkä and Arno Solin. *Applied Stochastic Differential Equations*. Cambridge University Press, 2019.
- [38] Moritz Schauer, Frank Van Der Meulen, and Harry Van Zanten. Guided proposals for simulating multi-dimensional diffusion bridges. *Bayesian Analysis*, 12(2):443–471, 2017.
- [39] Yuyang Shi, Valentin De Bortoli, Andrew Campbell, and Arnaud Doucet. Diffusion Schrödinger Bridge

- Matching. In *Neural Information Processing Systems*, pages 62183–62223. Curran Associates, Inc., 2023.
- [40] Xuan Su, Jiaming Song, Chenlin Meng, and Stefano Ermon. Dual Diffusion Implicit Bridges for Image-to-Image Translation. In *The Eleventh International Conference on Learning Representations*, 2023.
- [41] Patricia L. Suárez, Angel D. Sappa, Boris X. Vintimilla, and Riad I. Hammoud. Near InfraRed Imagery Colorization. In *2018 25th IEEE International Conference on Image Processing (ICIP)*, pages 2237–2241, 2018.
- [42] Aaron van den Oord, Yazhe Li, and Oriol Vinyals. Representation Learning with Contrastive Predictive Coding, 2019.
- [43] Haixia Wang, Zhigang Zhang, Zhanyi Hu, and Qilei Dong. SAR-to-Optical Image Translation With Hierarchical Latent Features. *IEEE Transactions on Geoscience and Remote Sensing*, 60:1–12, 2022.
- [44] Zihao Wang, Yuzhou Chen, and Shaogang Ren. Adaptive Domain Shift in Diffusion Models for Cross-Modality Image Translation. In *The Fourteenth International Conference on Learning Representations*, 2026.
- [45] Bohan Xiao, Peiyong Wang, Qisheng He, and Ming Dong. Deterministic Image-to-Image Translation via Denoising Brownian Bridge Models with Dual Approximators. In *Proceedings of the IEEE/CVF Conference on Computer Vision and Pattern Recognition*, pages 28232–28241, 2025.
- [46] Kaitao Xue, Bo Li, Ziyi Liu, Zhifen He, Bin Liu, Congxuan Zhang, and Yu-Kun Lai. BiBBDM: Bidirectional Image Translation With Brownian Bridge Diffusion Models. *IEEE Transactions on Pattern Analysis and Machine Intelligence*, 47(11):10546–10559, 2025.
- [47] Xi Yang, Haoyuan Shi, Ziyun Li, Maoying Qiao, Fei Gao, and Nannan Wang. S3OIL: Semi-Supervised SAR-to-Optical Image Translation via Multi-Scale and Cross-Set Matching. *IEEE Transactions on Image Processing*, 34:6641–6654, 2025.
- [48] Xi Yang, Haoyuan Shi, Zihan Wang, Nannan Wang, and Xinbo Gao. CSHNet: A Novel Information Asymmetric Image Translation Method. *IEEE Transactions on Circuits and Systems for Video Technology*, 36(2):1862–1875, 2026.
- [49] Sihyun Yu, Sangkyung Kwak, Huiwon Jang, Jongheon Jeong, Jonathan Huang, Jinwoo Shin, and Saining Xie. Representation Alignment for Generation: Training Diffusion Transformers Is Easier Than You Think. In *The Thirteenth International Conference on Learning Representations*, 2025.
- [50] Richard Zhang, Phillip Isola, and Alexei A. Efros. Colorful Image Colorization. In *Computer Vision – ECCV 2016*, pages 649–666, Cham, 2016. Springer International Publishing.
- [51] Richard Zhang, Phillip Isola, Alexei A. Efros, Eli Shechtman, and Oliver Wang. The Unreasonable Effectiveness of Deep Features as a Perceptual Metric. In *Proceedings of the IEEE Conference on Computer Vision and Pattern Recognition*, pages 586–595, 2018.
- [52] Bingxuan Zhao, Chuang Yang, Qing Zhou, and Qi Wang. RLI-DM: Robust Layout-Based Iterative Diffusion Model for SAR-to-RGB Image Translation. *IEEE Transactions on Geoscience and Remote Sensing*, 63:1–9, 2025.
- [53] Wenbo Zhao, Nana Jiang, Xiaoxin Liao, and Jubo Zhu. HVT-cGAN: Hybrid Vision Transformer cGAN for SAR-to-Optical Image Translation. *IEEE Transactions on Geoscience and Remote Sensing*, 63:1–17, 2025.
- [54] Kaiwen Zheng, Guande He, Jianfei Chen, Fan Bao, and Jun Zhu. Diffusion Bridge Implicit Models. In *The Thirteenth International Conference on Learning Representations*, 2025.
- [55] Linqi Zhou, Aaron Lou, Samar Khanna, and Stefano Ermon. Denoising Diffusion Bridge Models. In *The Twelfth International Conference on Learning Representations*, 2024.
- [56] Jun-Yan Zhu, Taesung Park, Phillip Isola, and Alexei A. Efros. Unpaired Image-To-Image Translation Using Cycle-Consistent Adversarial Networks. In *Proceedings of the IEEE International Conference on Computer Vision*, pages 2223–2232, 2017.

A Qualitative Results

B Per-Task Architectural Configurations

We provide the complete architectural and training specifications for each MAVIC-T task. [Tab. 4](#) summarizes DBIM hyperparameters (VP schedule, Karras ρ , base channels, etc.) for SAR→EO, SAR→RGB, and RGB→IR, as well as CUT settings for SAR→IR. Training resolution is 256×256 for SAR→EO and 512×512 for the 1024px tasks; full-resolution inference follows the approach described in [Sec. 6.1](#).

C Lessons and Insights

We summarize key lessons and insights from developing EarthBridge for the MAVIC-T translation track.

Diffusion Bridge vs. Standard Diffusion. The diffusion bridge directly builds a mapping from the source domain to the target domain, whereas standard diffusion starts from a noise prior (typically Gaussian noise) and requires a conditional generation strategy to accomplish this task. We hypothesize that the diffusion bridge is more efficient for training and achieves better results for cross-modal translation. However, standard diffusion can be more flexible for further conditional development, e.g., leveraging pre-trained models for a good prior. There is a trade-off between these approaches; we encourage readers to further explore both directions.

Resolution Scaling and Multi-Stage Curriculum. For 1024px modeling, we train on 512px only and directly infer on 1024px, which yields strong results while saving training compute budget. If time permits, we may further perform a quick fine-tuning on 1024px directly—we term this approach *multi-stage resolution curriculum learning*.

Task Difficulty and Input Modality. We found that SAR→EO and RGB→IR are substantially easier than the other two tasks. For RGB→IR, the three-channel input provides sufficient information for the translation. For

SAR→EO, the relative ease may stem from both modalities originating from the same sensor, reducing the domain gap.

Inference Steps and Metric Trade-offs. Using the DBIM ODE solver, few-step inference yields visually appealing results. For RGB→IR, even a single-step generation is sufficient, and increasing steps tends to hallucinate details. In practice, however, many more inference steps greatly improve FID and LPIPS in the competition metrics, even when L1 remains unchanged—highlighting a trade-off between perceptual quality, metric optimization, and inference efficiency.

Table 4. Per-task architectural and training configurations. Top: DBIM settings for SAR→EO, SAR→RGB, and RGB→IR. Bottom: CUT settings for SAR→IR (ResNet-9block generator, 4-layer PatchGAN discriminator).

Configuration	SAR→EO	SAR→RGB	SAR→IR	RGB→IR
<i>DBIM</i>				
Parameters	~20M	~120M	–	~120M
VP schedule (β_d, β_{\min})	2.0, 0.1	2.0, 0.1	–	2.0, 0.1
Karras ρ	7	7	–	7
Base channels	64	96	–	128
Channel multipliers	(1,2,3,4)	(1,1,2,2,4,4)	–	(1,1,2,2,4,4)
Attention resolutions	N/A	32, 16, 8	–	32, 16, 8
Training resolution	256 ²	512 ²	–	512 ²
Epochs	55	24	–	86
<i>CUT</i>				
Parameters (total)	–	–	~225M	–
Generator; Discriminator	–	–	~180M; ~45M	–
Generator (ResNet blocks)	–	–	9	–
Discriminator	–	–	4-layer PatchGAN	–
Filters (ngf, ndf)	–	–	256	–
GAN objective	–	–	LSGAN	–
$\tau, \lambda_{\text{GAN}}, \lambda_{\text{NCE}}$	–	–	0.1, 0.5, 1.0	–
Identity NCE	–	–	disabled	–
Training resolution	–	–	512 ²	–
Epochs	–	–	11	–

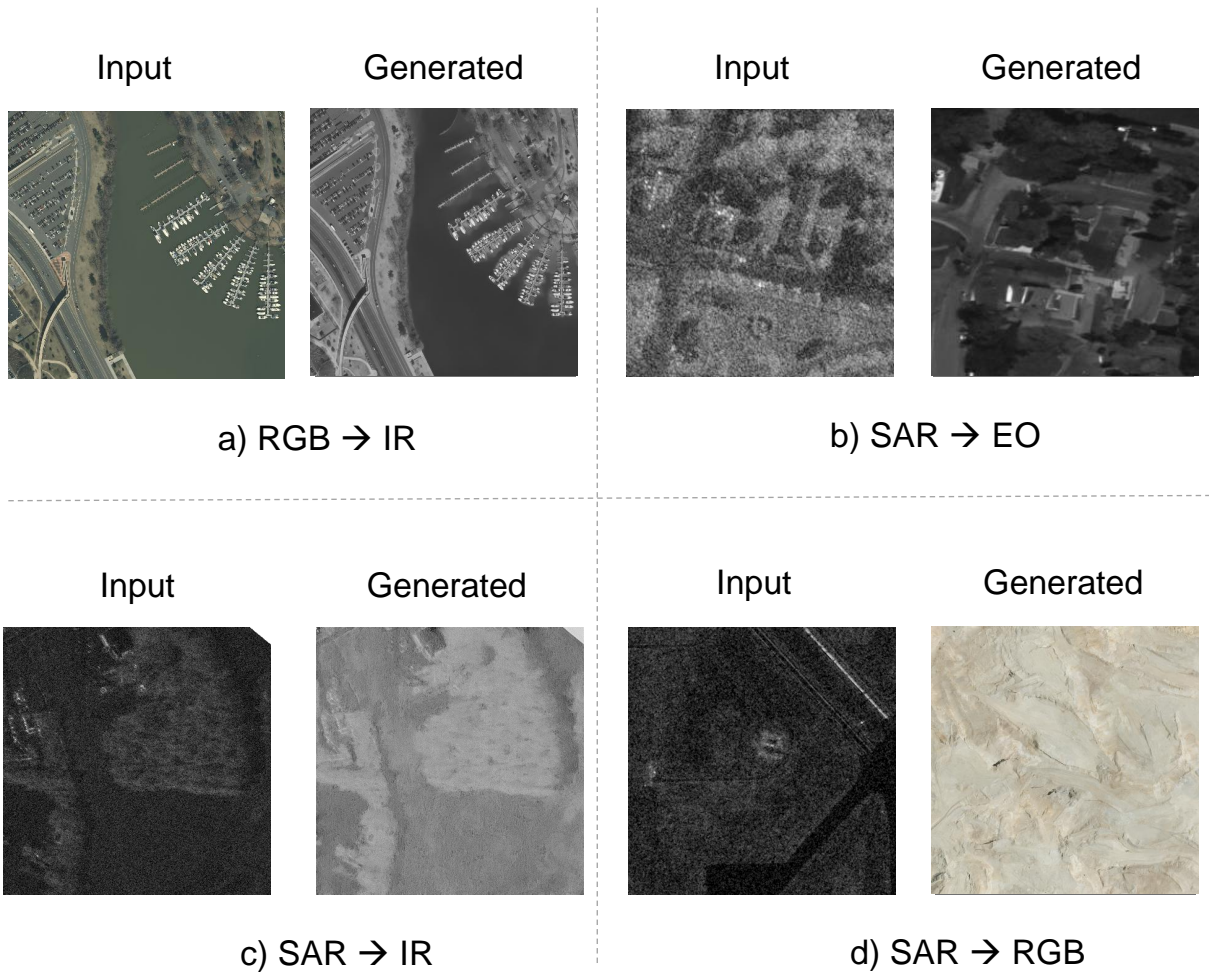


Figure 5. Qualitative results across all four MAVIC-T translation tasks. Each row corresponds to one task (SAR \rightarrow EO, SAR \rightarrow RGB, SAR \rightarrow IR, RGB \rightarrow IR). Columns show: source image, EarthBridge output, and ground-truth target. Our model preserves structural layout from the source while synthesizing faithful target-modality textures across both 256 \times 256 and 1024 \times 1024 resolutions.